Journal of Statistical Physics, Vol. 86, Nos. 3/4, 1997

Nonequilibrium Phase Transitions in a Simple Three-State Lattice Gas

G. Korniss,[1] B. Schmittmann,[1] and R. K. P. Zia[1]

Received April 1, 1996

We investigate the dynamics of a three-state stochastic lattice gas consisting of holes and two oppositely "charged" species of particles, under the influence of an "electric" field at zero total charge. Interacting only through an excluded-volume constraint, particles exchange with holes and, on a slower time scale, with each other. Using a combination of Monte Carlo simulations and mean-field equations of motion, we study a set of suitably defined order parameters, their histograms and fluctuations, as well as the current through the system. With increasing particle density and drive, the system first orders into a charge-segregated state, and then disorders again near complete filling. The transition is first order at low densities and turns second order at higher ones. The finite-size and aspect-ratio dependence of characteristic quantities is discussed at the mean-field level.

KEY WORDS: Driven lattice gas; order-disorder transition; Monte Carlo simulations; mean-field equations of motion; slow mode; adiabatic elimination.

1. INTRODUCTION

The art and science of modeling of physical systems in nonequilibrium steady states have attracted considerable attention in the past decade. Driven stochastic lattice gases are among the simplest ones in which the statistical mechanics of such steady states can be studied.[1] The "standard model," introduced over a decade ago by Katz *et al.*[2] is an Ising lattice gas with *periodic boundary conditions* subjected to a hopping dynamics in the presence of a uniform external "field" which favors (suppresses) jumps along (against) a particular direction on the lattice. Through Monte Carlo simulations, this system (at half filling) was shown to undergo a continuous

[1] Center for Stochastic Processes in Science and Engineering and Department of Physics, Virginia Polytechnic Institute and State University, Blacksburg, Virginia 24061-0435.

0022-4715/97/0200-0721$12.50/0

transition, at a field dependent temperature, from a disordered to a phase-segregated steady-state configuration. Theoretical understanding of these results is severely limited by the lack of Boltzmann-like factors which describe such stationary, but nonequilibrium, states. Nevertheless, *dynamic* field-theoretic renormalization group techniques[3] can be applied so that the critical properties associated with the second-order transition can be computed. The fixed point is non-Hamiltonian and is best displayed as a dynamic functional.[4] A number of the critical exponents, distinct from those in the Ising universality class, are confirmed by simulations.[5] A recent review of this early model, as well as the multitude of variations can be found in Ref. 1.

One natural generalization of the "standard model" is a lattice gas of more than one species of particles. The motivations come from both theoretical interests and physical systems. Examples of the latter range from fast ionic conductors with several mobile species[6] and water droplets in microemulsions with distinct charges[7] to gel electrophoresis[8] and traffic flow.[9] From a theoretical viewpoint it is of great interest to study the effects of external drives on not just the Ising model, but models with rich equilibrium phase structures, e.g., Potts,[10] Ashkin–Teller,[11] Blume–Emery–Griffiths,[12] ANNNI,[13] etc. In this paper we will focus on one of the simplest possibilities where only two species of particles, driven in opposite directions, are present.[14, 15] There are *no* interparticle interactions apart from a strict excluded-volume constraint. If the drive is absent, this model consists of simple diffusion into the totally random equilibrium state. Once the drive is turned on, however, an interesting phase diagram emerges, even for a system restricted to particle–hole exchanges and equal numbers of the two species.[14, 16] In particular, for low particle densities and drives, the system settles into a homogeneous disordered state with a high steady-state current. If either parameter is increased, the system undergoes a transition into an inhomogeneous state, with a small current. Here, one species blocks the progress of the other species and "gridlock" occurs.

In this paper we explore the effects on both the phase transition and the ordered states if the particles are also allowed to exchange among themselves. If we interpret the action of the drive on the particles as an external "electric" field on oppositely "charged" particles, then we may refer to this new process as "charge-exchange." In particular, we will introduce the ratio γ, which is the rate of charge exchanges relative to particle–hole exchanges. To model ions of different species,[6] γ should be vanishingly small. On the other hand, to model charged water droplets,[7] we are obliged to let γ be large, since charges move between droplets much faster than diffusion of the droplets. Since we will restrict ourselves to the non-interacting case, we do not expect any interesting phase transitions in the

large-γ limit, though that system may display anomalous diffusion.[17] Therefore, we will explore only the $\gamma < 1$ regime. We should mention that in *one dimension* the steady-state distribution of our model is known analytically.[18] Further, systems with *open boundaries* display the unexpected phenomenon of spontaneous symmetry breaking.[19] Our interest focuses on higher dimensions, in which richer critical phenomena typically take place.

In the next section we define the microscopic model and give some details of the MC simulations. In Section 3, we report the main simulation results: the extension of the density-field phase diagram in ref. 14 to a third dimension, i.e., γ. Theoretical understanding of the shape and nature of the order-disorder phase boundary, the subject of Section 4, is achieved within a mean-field approach. In a final section, we conclude with a brief summary and some open questions.

2. THE MICROSCOPIC MODEL AND ORDER PARAMETERS

We consider a square lattice of $L_\perp \times L_\parallel$ sites with periodic boundary conditions. Each site can be empty or occupied by either a positive or a negative particle. Therefore we define two occupation variables n^+_{xy} and n^-_{xy} in the usual way, i.e., assuming the values 1 or 0 depending, respectively, on the number of positive and negative particles at site (x, y). Our model is "noninteracting" in the sense, that apart from this excluded volume constraint, there are no other interparticle interactions. In particular, though we refer to these particles as "charged," they do not interact via the usual Coulomb potential. The charges couple only to the external drive, which we refer to as an "electric" field. We choose this field to be uniform in both space and time, with magnitude E and directed along the $+y$-axis.

In the absence of the drive the dynamics does not distinguish between species. A particle can randomly hop to a nearest neighbor empty site with a rate Γ. In addition, if a nearest neighbor site is occupied by an oppositely charged particle, they may exchange with rate $\gamma\Gamma$. Since charge is the only attribute of the particles, the latter process is also referred to as "charge exchange." In the presence of the field the rates of moving against the force will be suppressed exponentially.

For our simulations, we set $\Gamma = 1$, randomly choose a nearest neighbor pair of sites and exchange their contents according to the following rules:

(i) If one site is occupied and the other is empty, the exchange occurs with probability

$$W_{ph} = \min\{1, e^{q \cdot \delta y \cdot E}\} \tag{1a}$$

where q is the charge of the particle ($q = \pm 1$) and δy is the change in the y coordinate of the particle due to the jump.

(ii) If the two sites are occupied by opposite charges, a particle–particle exchange (or charge transfer) is attempted with the probability

$$W_{pp} = \gamma \cdot \min\{1, e^{\delta y \cdot E}\} \tag{1b}$$

where now δy is the change in the y coordinate of the *positive* particle due to the jump. Needless to say, it is irrelevant whether exchange takes place or not if both sites carry identical content. Note that, *locally*, these Metropolis rates satisfy detailed balance. However, due to the periodic boundary conditions, the states we seek will not satisfy this condition. After $L_\perp \cdot L_\parallel$ random pairs have been chosen "time" is incremented by a Monte Carlo step (MCS).

The microscopic dynamics defined above clearly conserves the number of each species separately. These two conserved quantities may also be chosen to be the total particle number and the net charge, which we will associate with the terms "mass" and "charge," respectively. In the simulations, we restrict ourselves to systems with *zero net charge*, but vary the overall mass density:

$$\bar{m} \equiv \frac{1}{L_\perp L_\parallel} \sum_{x,\, y} [n^+_{xy} + n^-_{xy}]$$

Since an equal number of positive and negative charges are driven in opposite directions, the average mass current through the system vanishes. In contrast, the average charge current is highly nontrivial, distinguishing between ordered and disordered states. To summarize, we have three control parameters: $\bar{m}$, E, and γ. In addition, to investigate finite-size effects, we have used several system sizes: $L_\perp$ and $L_\parallel$.

This model can be described by $P[C, t]$, the probability of finding our system in the configuration $C \equiv \{n^+_{xy}, n^-_{xy}\}$ at time t. Its time evolution is governed by a master equation:

$$\frac{\partial}{\partial t} P[C, t] = \sum_{C'} \{ W(C' \to C)\, P[C', t] - W(C \to C')\, P[C, t] \} \tag{2}$$

where $W(C' \to C)$ is the transition rate from C' to C. Of course, C and C' can differ by just one nearest neighbor pair of occupation numbers, with W being one of the rates W_{ph} and W_{pp} specified above. Starting our model in some initial, e.g., random, configuration, we are interested in its behavior

in the $t \to \infty$ limit, where we expect it to reach a stationary state with distribution $P^*[C]$. Had we chosen boundary conditions suitable for inducing an equilibrium state (e.g., "brick wall"), $P^*[C]$ would be just the familiar Boltzmann factor. By imposing periodic boundary conditions, we expect a *nonequilibrium*, t-independent state, with violation of detailed balance in general:

$$W(C' \to C)\, P^*[C'] \neq W(C \to C')\, P^*[C] \tag{3}$$

In principle, finding $P^*[C]$ involves nothing more than solving a linear equation, (2), with 0 on the left. In practice, however, this is impossible, except for special values of $\bar{m}$, E and γ. These particular exceptions are:

(i) The $E = 0$ plane. This is an equilibrium, "noninteracting" system. The particles diffuse randomly, both densities are homogeneous and $P^* \propto 1$ is the trivial solution.

(ii) The $\bar{m} = 1$ plane, with $\gamma > 0$. Here there are no holes, so that charge exchange is the only dynamics. Relabeling negative charges as "holes" and positive charges as "particles," the system reduces to the biased diffusion of a single, noninteracting species. The steady-state is, though nonequilibrium, also known exactly:[20] $P^* \propto 1$. While the densities are again homogeneous, the current no longer vanishes here.

(iii) The $\gamma = 1$ plane. With equal rates $W_{ph} = W_{pp}$, a positive (negative) charge can no longer distinguish a negative (positive) particle from a hole. Thus, a positive (negative) particle experiences biased diffusion, slowed only by encounters with other positive (negative) particles, just as in the case of a single, noninteracting species, and spatial inhomogeneities are again impossible for either charge density. We can show that $P^* \propto 1$ holds as in case (ii).

(iv) Finally note that the $\bar{m} = 1$, $\gamma = 0$ line is singular in the sense that the system remains completely frozen in its initial configuration.

None of these cases displays nontrivial spatial structures. Interesting phenomena such as transitions to inhomogeneous steady states are typically found through Monte Carlo simulations of P^*. The spontaneous formation of spatial structures, resembling a single, transverse strip of predominantly positive charge, blocking a similar strip of mostly negative charge, with the rest of the lattice being nearly empty, is easily observed. However, a quantitative phase diagram can only be drawn if one or more suitable order parameters are defined and measured. Even though the steady-state currents are natural candidates, they are rather indirectly

related to the steady state being disordered or ordered. Thus, it is reasonable to focus on the average density profiles themselves. In the range of investigated aspect ratios $L_\perp/L_{||}$, inhomogeneities in the x (transverse) direction were never observed. Consequently, we focus on profiles averaged over x.

Instead of $n^\pm$, we find it more convenient to use the local hole and charge densities, defined as follows:

$$\phi_{xy} \equiv 1 - (n^+_{xy} + n^-_{xy}) \qquad \text{and} \qquad \psi_{xy} \equiv n^+_{xy} - n^-_{xy} \tag{4}$$

The corresponding profiles of interest are denoted by

$$\phi(y) = \frac{1}{L_\perp} \sum_x \phi_{xy} \qquad \text{and} \qquad \psi(y) = \frac{1}{L_\perp} \sum_x \psi_{xy} \tag{5}$$

Based on the latter, the quantity

$$Q \equiv \frac{1}{\bar{m} L_{||}} \left\langle \sum_y [\psi(y)]^2 \right\rangle \tag{6}$$

was used as an order parameter earlier,[14, 21] where $\langle \bullet \rangle$ denotes average over the run, to be specified precisely at the end of this section. It is clear that Q is unity for a completely ordered system and zero [actually, $O(1/L_\perp)$ due to finite-size effects] in the disordered, homogeneous state. Though Q served us well in signaling discontinuous transitions, we found that it is not very sensitive to the onset of continuous transitions. Indeed, this deficiency might explain why the second-order transition line in the $\gamma = 0$ model had not been detected, even though it was expected theoretically.[22] Here, due to $\gamma > 0$, we expect continuous transitions to play a more prominent role. Therefore, we seek an order parameter which is more sensitive to the onset of small spatial inhomogeneities. A natural choice, designed to single out a transverse strip, comes from the amplitude of the longest wavelength Fourier component of the profile, as in the single-species models.[5] Defining the transforms

$$\tilde{\phi}_{k_\perp k_{||}} \equiv \frac{1}{L_\perp L_{||}} \sum_{x,\, y} \phi_{xy} \cdot \exp\{ik_\perp x + ik_{||} y\} \tag{7a}$$

and

$$\tilde{\psi}_{k_\perp k_{||}} \equiv \frac{1}{L_\perp L_{||}} \sum_{x,\, y} \psi_{xy} \cdot \exp\{ik_\perp x + ik_{||} y\} \tag{7b}$$

we see that the relevant components of (5) are;

$$\Phi \equiv |\tilde{\phi}_{0,\,2\pi/L_{||}}| \qquad \text{and} \qquad \Psi \equiv |\tilde{\psi}_{0,\,2\pi/L_{||}}| \tag{8}$$

From (6) it is clear that Q is the sum over all modes $\tilde{\psi}_{0,\,k_{||}}$, while Ψ is only the lowest one. As we will show in Section 4, in a mean field approach, only this one mode becomes soft near a continuous transition. In this sense, the signal of such a transition is expected to be "clean" in Ψ, but "diluted" in Q. In the next section we will see that the simulation data are entirely consistent with this picture.

To summarize, we choose $\langle \Phi \rangle$ and $\langle \Psi \rangle$ as order parameters. The average charge current density $\langle J \rangle$ is also studied, as in ref. 14. To find these quantities, we simulate our model on both square and rectangular shapes, with $L_{\perp}$ and $L_{||}$ ranging from 20 up to 60. Near the transition line, runs are started from both random and completely ordered initial configurations. Elsewhere in the phase diagram, runs are started from random configurations. To map out the phase diagram, we perform runs of 10^5 MCS (Monte Carlo steps per site), discarding the first 20 K MCS, to ensure that the system has reached steady state (which typically, occurs already after 10 K MCS). Data are then taken after every 100 MCS. To analyze the nature of the transitions, we perform longer runs (5×10^5 MCS), discarding the first 62.5 K MCS and sampling after every 125 MCS. These measurements are then averaged over a run to give $\langle \bullet \rangle$.

3. MONTE CARLO RESULTS

The phase diagram in $(\bar{m}, E, \gamma)$ space has been investigated in some detail at three different γ's: 0.02, 0.2, and 0.4, using 30×30 lattices (Fig. 1). For small values of $\bar{m}$ and E, typical steady-state configurations are disordered, characterized by homogeneous densities and large charge current $\langle J \rangle$. For sufficiently large values of γ, specifically for $\gamma > \gamma_c \simeq 0.62$, the system remains in this phase for all $(\bar{m}, E)$. In contrast, for smaller γ the excluded volume constraint dominates the charge-exchange mechanism and spatial inhomogeneities develop in both charge and mass density as E is increased beyond a mass- and γ-dependent threshold $E_c(\bar{m}, \gamma)$, shown as the U-shaped curves in Fig. 1. The particles gather into a single strip, transverse to the field, while the rest of the lattice remains essentially empty. The particle-rich strip itself is structured into two distinct regions: the "downstream" half is dominated by negative charges, while the "upstream" segment consists mostly of positive charges (inset of Fig. 1). Since the two types of charges impede each other, $\langle J \rangle$ is very small in this phase, which we will refer to as "ordered."

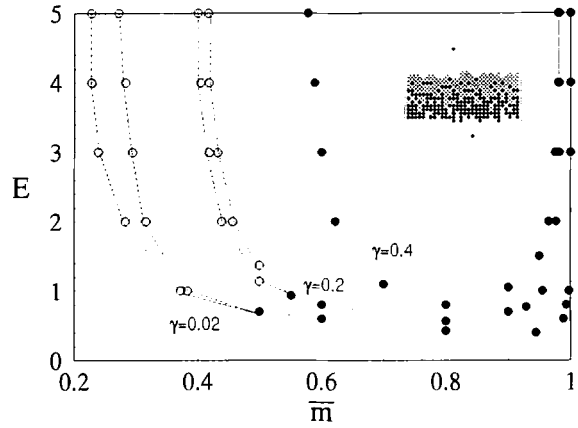

Fig. 1. Phase diagram for a 30×30 system in the $(\bar{m}, E)$ plane for three values of γ. The filled circles mark the lines of continuous transitions, while the open circles denote the spinodal lines associated with the first-order transitions. The inset shows a typical ordered configuration at $E = 3.0$ and $\bar{m} = 0.4$. Phase diagrams for other system sizes are similar while all data collapse if E is replaced by the scaling variable $\delta \equiv 2L_{\parallel} \tanh(E/2)$.

3.1. Order Parameters, Currents, and Histograms

Focusing on the detailed nature of this order–disorder transition, we first describe the region of small γ (0.02 and 0.2), with mass density $\bar{m}$ less than a characteristic threshold $\bar{m}_0(\gamma)$. As we vary E across the transition line $E_c(\bar{m}, \gamma)$, we observe abrupt changes in $\langle \Phi \rangle$, $\langle \Psi \rangle$, and $\langle J \rangle$ (Figs. 2a, 2b), signaling a first-order transition. To confirm this assignment, we search for another distinct signal of this transition type, i.e., hysteresis. Starting from ordered (disordered) initial configurations, we perform a series of runs, decreasing (increasing) $\bar{m}$ through the transition region at fixed E. Both order parameters and the charge current exhibit hysteresis loops, marking the *local* stability boundaries of the two phases, under these conditions. An example is displayed in Fig. 2c. Needless to say, the width of the hysteresis region (shown hatched in Fig. 1 for runs of 10^5 MCS in a 30×30 system) will vary with system size and length of runs. To demonstrate that close to the transition a *finite* system will switch back and forth between the ordered and disordered states, the time trace of Φ was measured during long runs of 5×10^5 MCS (Fig. 3a). To ease the "unlocking" of ordered configurations, a rather small value of E was chosen, so that jumps against the field occur with significant probability. The associated histogram for the order parameter Φ exhibits two well-separated peaks (Fig. 3b), corresponding to the two phases. These findings clearly

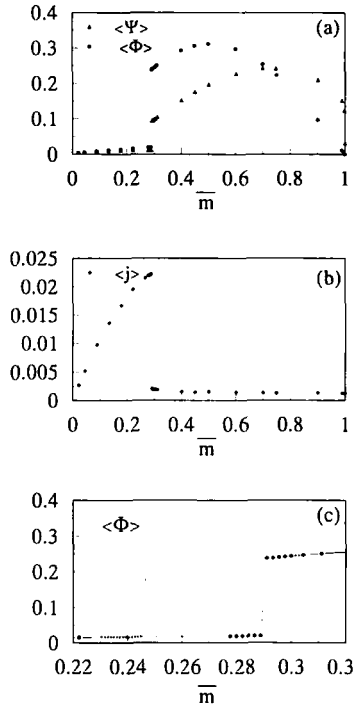

Fig. 2. Typical observables as functions of density ($\bar{m}$) near the first-order transition for a 30×30 system at $E = 3.0$ and $\gamma = 0.02$. In (a) and (b), runs are started from initially random configurations. (a) Order parameters $\langle \Phi \rangle$ and $\langle \Psi \rangle$. (b) Conductivity $\langle j \rangle \equiv \langle J \rangle / \varepsilon$. (c) Hysteresis loop across the first-order transition. Open (closed) circles refer to runs started from ordered (random) initial configurations.

support the transition being first order in this region, similar to the $\gamma = 0$ case.[14] Unfortunately, lacking an equivalent of the equilibrium free energy here, we cannot establish the precise location of the transition line without considerable computational effort.

As $\bar{m}$ increases, the hysteresis loops exhibited by $\langle \Phi \rangle$, $\langle \Psi \rangle$, and $\langle J \rangle$ shrink, becoming unobservable for $\bar{m} \geqslant \bar{m}_0(\gamma)$. Instead, the order parameters $\langle \Phi \rangle$ and $\langle \Psi \rangle$ vary continuously (Fig. 4) upon crossing the line $E_c(\bar{m}, \gamma)$, typical of a second-order rather than first-order, transition. The nonzero values at small E are due entirely to finite-size effects, being of $O((L_\perp L_{||})^{-1/2})$. Unlike the $\bar{m} < \bar{m}_0$ case above, the histograms for Φ show a single peak, which moves smoothly away from the origin as the transition line is crossed (Fig. 5). At the transition, the distribution broadens considerably (Fig. 5c), reflecting an increase in the order

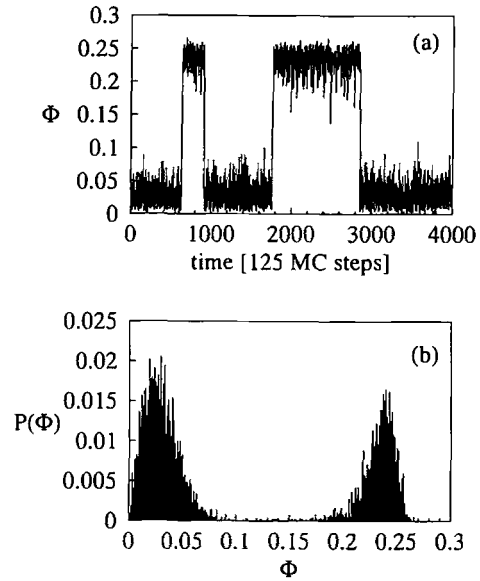

Fig. 3. Time trace (a) and histogram (b) for the order parameter $\langle \Phi \rangle$ at $E = 1.0$, $i\bar{m} = 0.38$, and $\gamma = 0.02$ for a 30×30 system.

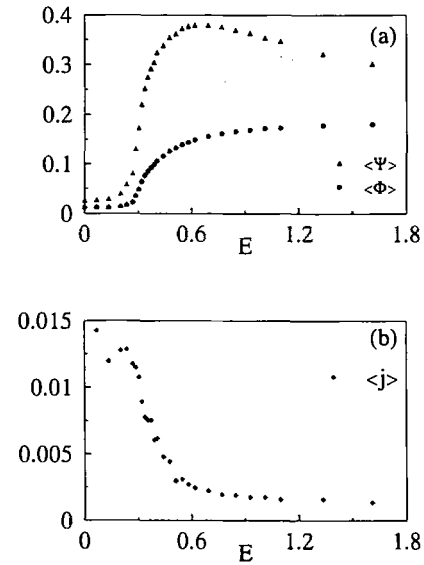

Fig. 4. Typical observables as functions of E near the continuous transition for a 30×30 system at $i\bar{m} = 0.80$ and $\gamma = 0.02$. Runs started from initially random or ordered configurations collapse onto the same curve. (a) Order parameters $\langle \Phi \rangle$ and $\langle \Psi \rangle$. (b) Conductivity $\langle j \rangle \equiv \langle J \rangle / \varepsilon$.

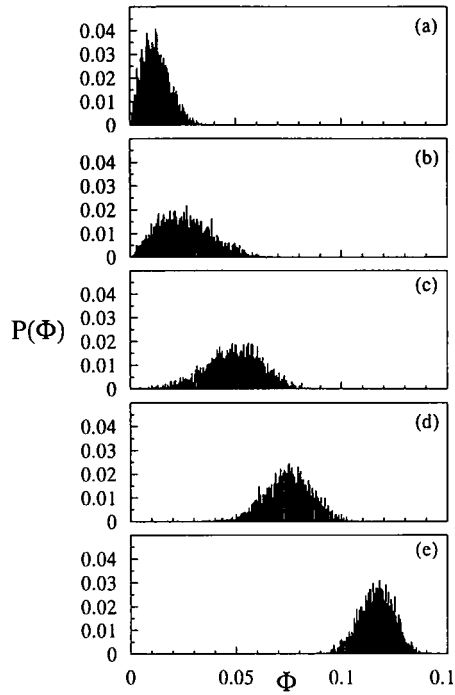

Fig. 5. Histograms for order parameter $\langle \Phi \rangle$ near the second-order transition for a 30×30 system at $\bar{m} = 0.80$ and $\gamma = 0.02$, for a series of E: (a) $E = 0.13$; (b) $E = 0.27$; (c) $E = 0.30$; (d) $E = 0.34$; (e) $E = 0.44$.

parameter fluctuations. These data strengthen our believe that this transition is second order in nature.

To investigate the transition in more detail, we perform long (5×10^5 MCS) runs on a series of rectangular lattices, focusing on $\langle \Phi \rangle$, its fluctuations $\langle (\Delta \Phi)^2 \rangle$, and $\langle J \rangle$, at several values of E, just above and below the transition, keeping γ and $\bar{m}$ fixed. Anticipating a result from the mean-field theory analysis (Section 4), we plot our data versus the scaling variable $\mathscr{E} \equiv \varepsilon L_{||}$, where $\mathscr{E} = 2 \tanh(E/2)$ is the "coarse-grained' field. We should emphasize that our objective here is, first, to confirm the existence of a continuous transition, and second, to gain initial insights into the finite-size and aspect-ratio dependence of characteristic quantities. We do not attempt, at this point, to measure, e.g., critical indices. The latter endeavor would require a detailed finite-size scaling analysis, focused on the critical region, where we may expect to observe deviations from the simple mean-field scaling adopted above. Currently, such a quantitative analysis is severely hampered by the absence of reliable field

theory predictions for the leading universal scaling behavior of our model.

Returning to the data, Fig. 6 shows our results for lattices with $L_{||}=20$ fixed and $L_{\perp}=20$, 40 and 60, while Fig. 7 corresponds to $L_{\perp}=20$, 40 and 60 with $L_{\perp}$ fixed at 20. With the exception of a finite-size tail, $\langle \Phi \rangle$ is essentially independent of $L_{\perp}$, depending on $L_{||}$ only through $\mathscr{E}$ (Figs. 6a, 7a). From these figures we see that the critical point occurs at $\mathscr{E}_c \simeq 9.0$. Keeping the limited accuracy of our data in the critical region in mind, a log–log plot of $\langle \Phi \rangle$ versus $|\mathscr{E}-\mathscr{E}_c|$ yields a first estimate for the order parameter exponent $\beta \sim 0.4$. A good indication for the presence of a continuous transition is provided by the fluctuations $\langle (\Delta\Phi)^2 \rangle$ (Figs. 6b, 7b), normalized to 1 in the fully random phase ($E=0$). Again, the data collapse quite well. While the height of the peak centered around $\mathscr{E}_c$ appears to be only weakly dependent on $L_{||}$ (Fig. 7b), it increases

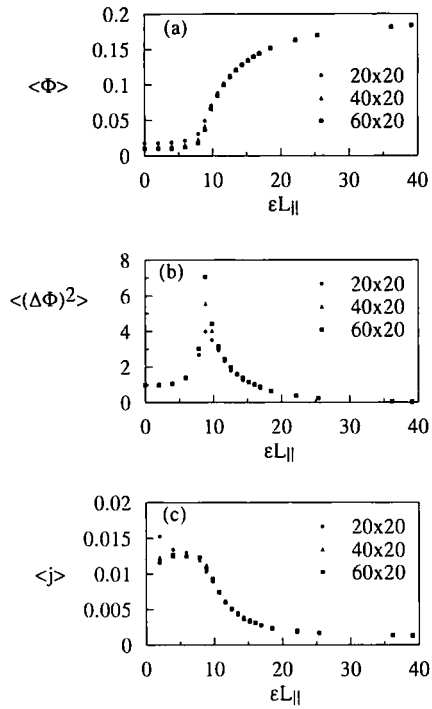

Fig. 6. Characteristic observables as functions of $\delta = \varepsilon L_{||}$ near the continuous transition for an $L_{\perp} \times L_{||}$ system with $L_{||}=20$ and $L_{\perp}$ ranging from 20 to 60, at $\bar{m}=0.80$ and $\gamma=0.02$: (a) Order parameter $\langle \Phi \rangle$; (b) Normalized order parameter fluctuations $\langle (\Delta\Phi)^2 \rangle$; (c) Conductivity $\langle j \rangle$.

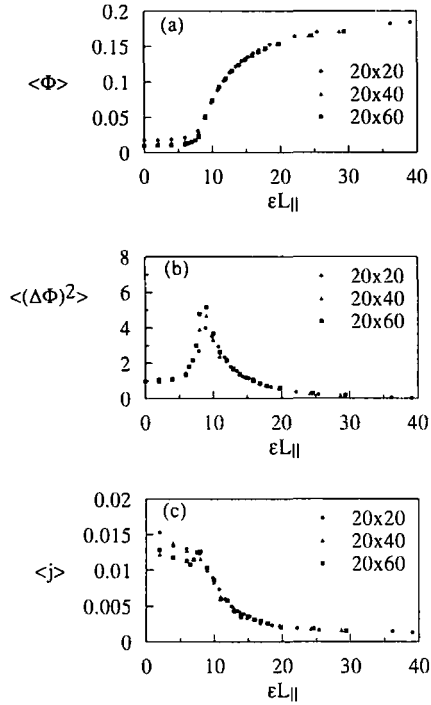

Fig. 7. Characteristic observables as functions of $\delta = \varepsilon L_{||}$ near the continuous transition for an $L_\perp \times L_{||}$ system at $\bar{m} = 0.80$ and $\gamma = 0.02$. Here $L_\perp = 20$ and $L_{||}$ ranges from 20 to 60: (a) Order parameter $\langle \Phi \rangle$; (b) Normalized order parameter fluctuations $\langle (\Delta\Phi)^2 \rangle$; (c) Conductivity $\langle j \rangle$.

significantly with $L_\perp$ (Fig. 6b). This intriguing size dependence is borne out by our theoretical analysis (Section 4). Finally, we focus on the conductivity $\langle j \rangle \equiv \langle J \rangle / \varepsilon$. Fluctuating about a constant value in the disordered phase, it appears to exhibit a discontinuity in its slope, upon crossing the transition line into the ordered region. Beyond the transition, it decreases monotonically, approaching a small limiting value deep in the ordered phase. This value is proportional to γ, which fits well with the picture that particle–hole exchanges are rare in this regime and $\langle J \rangle / \varepsilon$ is dominated by the charge exchange mechanism. To summarize, all of these characteristics are consistent with the scenario of a continuous transition. Clearly, the scaling of the critical parameter, δ_c with the longitudinal system size $L_{||}$ is crucial: for $L_{||} \to \infty$, the transition shifts to $E = 0$.

For $\gamma = 0.2$ the behavior of the system is qualitatively similar to the case $\gamma = 0.02$. The major differences are as follows.

(i) Since larger γ favors the disordered phase, the whole transition line is shifted upwards.

(ii) The region between the spinodals is narrower.

(iii) The point $\bar{m}_0(\gamma)$ shifts to slightly higher densities.

(iv) Finally, there appears to be a *finite* region of disorder for all E, just below complete filling.

Concerning the last point, we have some further remarks. Clearly, the plane $\bar{m} = 1$ itself must be disordered, given that the associated steady-state distribution is homogeneous. However, for $\gamma = 0.02$, $E \gtrsim 3.0$ and $L_\perp = L_\parallel = 30$, the removal of just two particles suffices to induce spatial inhomogeneities, with the two holes performing a random walk which leaves a charge-segregated region in its wake. For $\gamma = 0.2$, on the other hand, the system remains disordered until the density of holes exceeds 0.02 on a 30×30 lattice. We should caution, however, that considerably more work is required here before a reliable conclusion, concerning the details of the phase diagram near $\bar{m} = 1$ for different system sizes, can be reached.

Once γ has reached 0.4, $\bar{m}_0(\gamma)$ appears to have vanished, in that we no longer observe any indications of metastability or hysteresis. Thus, the line $E_c(\bar{m}_0(\gamma), \gamma)$, being a line of multicritical points, separates a surface of first-order transitions from a surface of continuous ones.

To complete the phase diagram, we also investigate the transition as γ varies, for fixed $(\bar{m}, E)$, in a system of size 30×30. Consistent with our previous findings for $E_c(\bar{m}_0(\gamma), \gamma)$, the order of the transition depends on where the orderly disorder transition surface is crossed. For $\gamma > \gamma_c \simeq 0.62$, the charge exchange mechanism suppresses the ordered phase entirely.

3.2. Density Profiles in the Ordered Phase

While the Fourier components $\langle \Phi \rangle$ and $\langle \Psi \rangle$ allow us to distinguish easily between the disordered and ordered phases, the full profiles $\phi(y)$ and $\psi(y)$ carry far more detailed information about the structure of the ordered phase itself. In particular, characteristic profiles measured near the first-order transition differ significantly from their counterparts near the continuous transition. Focusing on the ordered phase, just beyond the first-order transition line, the charge and hole density profiles are similar to those found in refs. 14 and 22 for $\gamma = 0$, i.e., the particle-rich strip exhibits three fairly sharp interfaces: two of these separate particles from holes at either end of the strip, while the third is located in the middle of the strip, marking the boundary between positive and negative charges (Fig. 8a). The hole density vanishes in the central region of the strip, so that the

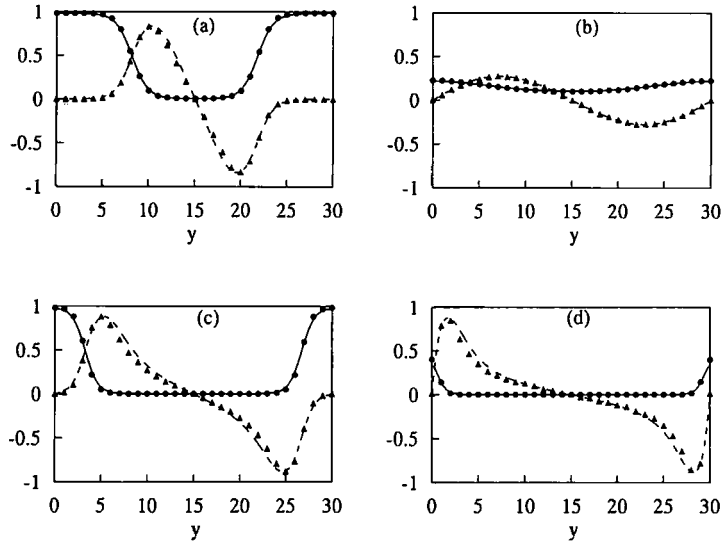

Fig. 8. Characteristic profiles in the ordered phase. Circles and triangles denote simulation results for the hole density profile $\phi(y)$ and the charge density profile $\psi(y)$, respectively. The system size is 30×30, $\gamma = 0.02$. Solid (dashed) lines are mean-field theory profiles for the hole (charge) density. (a) $\bar{m} = 0.46$, $E = 1.35$ ($\varepsilon L_{||} = 35.29$); (b) $\bar{m} = 0.84$, $E = 0.28$ ($\varepsilon L_{||} = 8.45$); (c) $\bar{m} = 0.78$, $E = 1.84$ ($\varepsilon L_{||} = 43.51$); (d) $\bar{m} = 0.98$, $E = 2.97$ ($\varepsilon L_{||} = 54.16$).

small residual current in this locked state is almost entirely due to charge exchange. In stark contrast, near the second-order line both charge and hole density profiles resemble harmonic functions, and the hole profile never vanishes, so that the system orders, but does not lock up fully (Fig. 8b).

Moving deeper into the ordered phase, one might expect to find profiles similar to Fig. 8a. Instead, for larger particle densities the central interface begins to soften, so that the strip, reminiscent of a sandwich, develops three, rather than two, regions: while its lower (upper) part still consists mainly of + (−) charges, there is now a distinct middle section which shows both species mixing by virtue of charge exchange (Fig. 8c). At the same time, the interfaces between particles and holes remain quite sharp. Finally, turning to ordered profiles near complete filling, the middle section of the strip has widened even further, bounded by two regions of either charge at the ends. Simultaneously, the two particle–hole interfaces have approached one another so closely that the few remaining holes are confined to just two or three rows. In fact, it is intriguing to track the dynamics of the ordering process here, starting from an initially random configuration: each hole acts as a catalyst for the charge segregation

process, creating a predominantly positive domain separated by a sharp interface from a similar, negatively dominated region located "upstream." For the system sizes considered here, these partially ordered regions quickly merge into a single strip, trapping the holes in the interfacial region (Fig. 8d). Further studies are in progress to provide a more quantitative understanding of the phase diagram near complete filling.

4. MEAN-FIELD THEORY

We now turn to the analytic description of our model, in order to develop a better understanding of the nature of the order–disorder transition discussed in the previous section. As already indicated, this also provides the framework in which first predictions, concerning, e.g., the size dependence of characteristic observables, can be made. Aiming toward universal properties, we will construct a set of coarse-grained equations of motion, in continuous space and time, for the two conserved densities in our system. While the master equation (2) is far too difficult to solve even for stationary states, it serves as a convenient starting point for this approach. A hierarchy of evolution equations for the densities and higher order correlations follows straightforwardly. The mean-field approximation consists in truncating higher order density–density correlations,[15] so that a closed set of equations for the densities alone result. Explicit stationary solutions to these equations, corresponding to spatially homogeneous and inhomogeneous steady states, will be found. A linear stability analysis around the former will be presented. Our goal is to establish a parallel to the simulation results. By associating stable homogeneous solutions with the disordered phase, and stable inhomogeneous ones with typical ordered configurations, we are able to predict the characteristic behavior of the order parameters, the currents, and the density profiles. Finally, using an adiabatic elimination procedure, we project out an equation of motion for the slow mode, resulting in an analytic expression for a "tricritical" line which separates first-order from continuous transitions. Since this analytic approach provides us with good qualitative agreement with simulation results, we believe that considerable insight into the nature of these transitions is gained.

4.1. Equations of Motion

Defining the average densities of positive and negative charges, $\langle n^{\pm}_{xy} \rangle_t \equiv \sum_C n^{\pm}_{xy} P[C, t]$, we obtain their equations of motion from

$$\partial_t \langle n^{\pm}_{xy} \rangle_t = \sum_C n^{\pm}_{xy} \partial_t P[C, t] \tag{9}$$

Exploiting the master equation (2) with the transition rates (1), we find that the right-hand side of (9) will contain correlations of many n's. The mean-field approximation consists of truncating these correlations and replacing $\langle n \cdots n \rangle$ by $\langle n \rangle \cdots \langle n \rangle$. As a result, (9) becomes a time evolution equation for $\langle n_{xy}^{\pm} \rangle$, alone. To simplify further, we take a naive continuum limit, so that $\langle n_{xy}^{\pm} \rangle \to \rho^{\pm}(\mathbf{r}, t)$, where the latter symbol denotes the particle densities in continuous space. Since these are both conserved, the resulting equations take the form of continuity equations, $\partial_t \rho^{\pm} + \nabla \mathbf{j}^{\pm} = 0$. Spatial derivatives up to second order are included, choosing unit lattice constant. We will also need the continuum versions of the hole and charge densities defined in (4), namely $\phi(\mathbf{r}, t) \equiv 1 - [\rho^{+}(\mathbf{r}, t) + \rho^{-}(\mathbf{r}, t)]$ and $\psi(\mathbf{r}, t) \equiv \rho^{+}(\mathbf{r}, t) - \rho^{-}(\mathbf{r}, t)$. It is further convenient to introduce the asymmetric gradient operator $\tilde{\nabla}$, defined via its action on two functions f and g, namely $f\tilde{\nabla}g \equiv f\nabla g - g\nabla f$. Extending our discussion to a d-dimensional system, with the drive acting only along the y direction, we must distinguish spatial derivatives along the parallel direction, denoted by ∂, from gradients restricted to the $(d-1)$ transverse directions, ∇. The presence of spatial anisotropy is then reflected in the form of the currents, $\mathbf{j}^{\pm} = -\mathbb{K}\nabla\mu^{\pm}$, where $\mu^{\pm}$ denotes a scalar "chemical" potential and $\mathbb{K}$ is a mobility *matrix* which is diagonal *without* being a simple multiple of the unit matrix. Instead, we find with an appropriate rescaling of an overall time scale[2] that $\nabla\mathbb{K}\nabla = \kappa\nabla^2 + \partial^2$, with $\kappa = 2/(1 + e^{-|E|})$. The resulting equations of motion now follow:

$$\partial_t \rho^{\pm} = -\nabla\mathbb{K}\{[\rho^{\pm}\tilde{\nabla}\phi \pm \varepsilon\hat{y}\rho^{\pm}\phi] + \gamma[\rho^{\pm}\tilde{\nabla}\rho^{\mp} \pm \varepsilon\hat{y}\rho^{\pm}\rho^{\mp}]\} \tag{10}$$

Here, $\hat{y}$ is a unit vector along the y direction, so that $\varepsilon\hat{y}$ captures the effect of the drive, in our mean-field description. Its amplitude can be obtained explicitly from the microscopic rates (1) as

$$\varepsilon = 2\tanh(E/2) \tag{11}$$

Equations (10) manifest the equivalent structure of particle–hole and charge exchanges, the ratio of the associated rates being γ. Setting $\gamma = 0$, we recover the equations of motion first proposed in ref. 14 for a model without charge exchange. Thus, the second term in the $\{\ldots\}$ brackets, being proportional to γ, models the new process. The full expressions under the $\{\ldots\}$ brackets are just the current densities $\mathbf{j}^{\pm}$ of the $+(-)$ particles. One way to arrive at (10) is, in fact, through postulating reasonable constituent forms for the current.

[2] As a consequence of this rescaling, the mean-field "time" differs from the MC "time" by a factor $1/\kappa$. To ease comparison with analytic results, our MC data for the current $\langle J \rangle$ have been normalized by this factor, which improves the data collapse in Fig. 6c significantly.

Equations (10) may also be regarded as the "coarse-grained" version of the microscopic dynamics, especially if we add Langevin noise terms.[23] In this sense, they play the same role for our model as the Landau–Ginzburg Hamiltonian for the Ising model. The important symmetry here, under the combined operation $\rho^{\pm} \to \rho^{\mp}$ and $\varepsilon \to -\varepsilon$ is evident.

A helpful, alternate perspective of (10) can be gained by using, instead of ρ^+ and ρ^-, the hole and charge densities $\phi(\mathbf{r}, t)$ and $\psi(\mathbf{r}, t)$, respectively. Their time evolutions are governed by

$$\partial_t \phi = \nabla \mathbb{K} \{ \nabla \phi + \varepsilon \hat{y} \phi \psi \} \tag{12a}$$

$$\partial_t \psi = \nabla \mathbb{K} \left\{ \gamma \nabla \psi + (1-\gamma)\, \phi \tilde{\nabla} \psi - \varepsilon \hat{y} \phi (1-\phi) - \frac{\gamma}{2} \varepsilon \hat{y} [(1-\phi)^2 - \psi^2] \right\} \tag{12b}$$

To complete the specification, we impose periodic boundary conditions (PBC) on the densities and constraints due to $\bar{m}$ and zero net charge:

$$\int d\mathbf{r}\, \phi(\mathbf{r}, t) = (1-\bar{m}) \cdot L_{\perp} L_{\parallel} \tag{13a}$$

and

$$\int d\mathbf{r}\, \psi(\mathbf{r}, t) = 0 \tag{13b}$$

Finally, to compare with simulations, we should set $d = 2$.

4.2. Homogeneous and Inhomogeneous Solutions

In this subsection we investigate the stationary solutions of Eqs. (12), i.e., solutions satisfying $\partial_t \phi = \partial_t \psi = 0$, subject to PBC and the constraints (13). By virtue of (13b), it is immediately clear that such solutions can carry no hole (or mass) current: since the densities of positive and negative charges are equal, the net mass current through any surface will vanish in the steady state. The charge current, on the other hand, can and will be nontrivial. Being continuity equations, Eqs. (12) are trivially satisfied by homogeneous hole and charge densities:

$$\phi(\mathbf{r}) \equiv 1 - \bar{m}, \qquad \psi(\mathbf{r}) \equiv 0 \tag{14a}$$

Inserting these into (12), we may identify the charge current density associated with these homogeneous solutions:

$$J_{//} = \varepsilon \left[\bar{m}(1-\bar{m}) + \frac{\gamma}{2} \bar{m}^2 \right] \tag{14b}$$

Thus, the conductivity $j_{II} \equiv J_{II}/\varepsilon$ is independent of ε. Comparing to Figs. 4b, 6c, and 7c, we note that this is approximately satisfied by our simulation results.

Next we demonstrate the existence of inhomogeneous solutions. To mirror typical ordered configurations, we seek solutions of the form $\phi(\mathbf{r}, t) \equiv \phi(y)$, $\psi(\mathbf{r}, t) \equiv \psi(y)$, displaying a spatial dependence in y only. Inserting this ansatz, we can integrate Eqs. (12) once. The integration constants are just the hole and charge current densities carried by $\phi(y)$ and $\psi(y)$. By symmetry, only the latter, denoted by J_I, can be nonzero. Rescaling the coordinate $y \to z \equiv \varepsilon y$ and introducing the conductivity $j_I \equiv J_I/\varepsilon$, we cast Eqs. (12) into the form:

$$0 = \phi' + \phi\psi \tag{15a}$$

$$-j_I = \gamma\psi' + (1-\gamma)(\phi\psi' - \psi\phi') - \phi(1-\phi) - \frac{\gamma}{2}[(1-\phi)^2 - \psi^2] \tag{15b}$$

where ϕ and ψ are simply functions of z, and the prime denotes differentiation with respect to z. Equation (15a) allows us to eliminate $\psi = -\phi'/\phi$ in favor of ϕ so that (15b) reduces to an ordinary second-order differential equation for ϕ. Unlike ref. 14, however, the substitution $\chi \equiv 1/\phi$ *does not* lead to an equation of potential form for χ''. Instead, suppressing the subscript on j, we obtain

$$\chi'' = [1 - \gamma + \gamma\chi]^{-1}\left\{-j\chi^2 + \chi - 1 + \frac{\gamma}{2}[(\chi-1)^2 + (\chi')^2]\right\} \tag{16}$$

which reduces to potential form only upon setting $\gamma = 0$. However, defining a new function $u(\chi(z))$ via

$$u \equiv \left(1 + \frac{\gamma}{1-\gamma}\chi\right)^{1/2} > 0 \tag{17}$$

we transform (16) into the desired form for all γ. Thus,

$$u'' = -\frac{d}{du}V(u) \tag{18a}$$

where

$$V(u) = \frac{j}{2\gamma}\left\{\frac{u^2}{2} - 2\ln u - \frac{1}{2u^2}\right\} - \frac{u^2}{8} - \frac{1}{8(1-\gamma)^2 u^2} \tag{18b}$$

By definition, χ is restricted to the interval $[1, \infty)$, whence $(1-\gamma)^{-1/2} \leqslant u < \infty$. In order to find periodic solutions for u which map into spatially inhomogeneous solutions for ϕ and ψ, $V(u)$ must possess a local minimum in that range. A simple analysis of (18b) shows that this is indeed the case for

$$\frac{\gamma}{2} < j < \frac{1}{4-2\gamma} \tag{19}$$

Since the potential $V(u)$ here is quite complex, the solutions of (18) cannot be found in closed form, unlike the $\gamma = 0$ model.[14, 22] However, the charge and hole density profiles can easily be obtained by numerical integration. As initial conditions, we choose a value for j in the range specified by (19), and set $u(0) \equiv u_0$, $u'(0) = 0$. To compare with a simulation, the integration constants u_0 and j must be mapped onto the microscopic control parameters $\bar{m}$, E, $L_\perp$ and $L_{||}$. To reduce the number of adjustable parameters, we simply set $L_\perp = L_{||} = 30$. Once a mean-field profile ϕ is obtained, we can determine, first, its overall mass density $\bar{m}$ via $\int dy\, \phi(y) = (1-\bar{m})\, L_{||}$, and second, its period $\varepsilon L_{||}$. The latter provides us with E, via Eq. (11), so that there are no fit parameters! The resulting profiles, obtained by numerical integration of our mean-field theory and simulation at the associated points in the phase diagram, are shown in Fig. 8. The agreement is impressive. In particular, near complete filling the profiles clearly reflect the localization of the hole density at the steep plus–minus interface. To conclude, we note that small deviations from the Monte Carlo data are confined to the regions of largest ϕ' and ψ', and can be reduced further by including higher derivatives in (10), (12).

4.3. Linear Stability Analysis

Recalling the homogeneous solutions, we see that from Eq. (14) one such solution exists at *every* point of $(\bar{m}, \varepsilon)$ space. However, our mean-field analysis has not yet provided any insight into their *stability*, with respect to small perturbations. In order to explore this issue, we must return to the full time-dependent set of equations (10), (12). To investigate the evolution of a small harmonic perturbation about the homogeneous phase $\bar{\phi} \equiv 1 - \bar{m}$, $\bar{\psi} = 0$, we write

$$\phi(\mathbf{r}, t) = \bar{\phi} + \sum_{\mathbf{k} \neq 0} \tilde{\phi}(\mathbf{k}) \exp[-(\tau t + \mathbf{i}\mathbf{k} \cdot \mathbf{r})] \tag{20a}$$

$$\psi(\mathbf{r}, t) = \bar{\psi} + \sum_{\mathbf{k} \neq 0} \tilde{\psi}(\mathbf{k}) \exp[-(\tau t + \mathbf{i}\mathbf{k} \cdot \mathbf{r})] \tag{20b}$$

where $\mathbf{k} \equiv (k_\perp, k_{||})$ must be compatible with the periodic boundary conditions. Thus, in spatial dimension $d=2$, we let $(k_\perp, k_{||}) = (2\pi n/L_\perp, 2\pi m/L_{||})$ with integer n, m. Assuming small amplitudes $\tilde{\phi}(\mathbf{k})$ and $\tilde{\psi}(\mathbf{k})$, we may linearize (12). Defining

$$\xi(\mathbf{k}) \equiv \begin{bmatrix} \tilde{\phi}(\mathbf{k}) \\ \tilde{\psi}(\mathbf{k}) \end{bmatrix} \tag{21a}$$

we write the linearized equation as

$$\tau \xi(\mathbf{k}) = \mathbb{L}(\mathbf{k})\, \xi(\mathbf{k}) \tag{21b}$$

where the matrix $\mathbb{L}(\mathbf{k})$ is given by

$$\mathbb{L}(\mathbf{k}) = \begin{bmatrix} \mathbf{k}\mathbb{K}\mathbf{k} & ik_{||}\varepsilon\bar{\phi} \\ ik_{||}\varepsilon[\gamma(1-\bar{\phi}) - (1-2\bar{\phi})] & \mathbf{k}\mathbb{K}\mathbf{k}[\gamma(1-\bar{\phi}) + \bar{\phi}] \end{bmatrix} \tag{21c}$$

with $\mathbf{k}\mathbb{K}\mathbf{k} = \kappa k_\perp^2 + k_{||}^2$. The two eigenvalues of $\mathbb{L}(\mathbf{k})$ determine the two branches of the dispersion relation, $\tau = \tau_\pm(\mathbf{k})$, and from Eq. (21b) it is easy to see that the homogeneous phase remains stable with respect to small perturbations as long as the real part of $\tau_\pm(\mathbf{k})$ is positive for all $\mathbf{k}$. It is also easy to see that $\tau_\pm(k_\perp, k_{||}=0) \propto k_\perp^2 > 0$. Further, since $\tau_\pm(k_\perp, k_{||}) > \tau_+(0, k_{||})$ and the most relevant perturbation is the one associated with the smallest eigenvalue, we need to focus only on the $k_\perp = 0$ modes. Not surprisingly, among this set, the slowest mode is associated with the lowest wave vector, i.e., $k_{||} = 2\pi/L_{||}$. Setting $\tau_-(0, 2\pi/L_{||}) = 0$ we thus find the first onset of instability. The result is that a specific homogeneous solution with mass density $\bar{m}$ will become unstable when ε exceeds a critical $\varepsilon_{//}(\gamma, \bar{m})$ given by

$$\varepsilon_{//} L_{||} = 2\pi \left\{ \frac{1 - \bar{m} + \gamma\bar{m}}{(1-\bar{m})[(2-\gamma)\,\bar{m} - 1]} \right\}^{1/2} \tag{22}$$

Since (22) is real only in the range $1/(2-\gamma) \equiv \bar{m}_{\min}(\gamma) < \bar{m} < 1$ and diverges at the endpoints, the homogeneous solutions are stable outside this interval. In particular, if $\gamma \geqslant 1$, they are always stable. For three smaller values of γ the resulting linear stability boundary is plotted in Fig. 9. Since we have neglected nonlinear terms as well as fluctuations, we cannot identify Eq. (22) directly with the observed phase boundary (Fig. 1). However, it does mirror the shape of the transition line surprisingly well, and predicts, in particular, the vanishing of the ordered phase beyond a critical γ_c.

Of course, a linear stability analysis cannot provide us with information on the nature of the phase transition. In particular, if the transition is

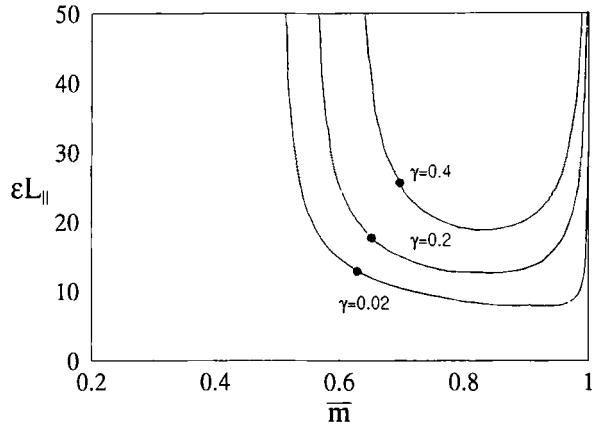

Fig. 9. Mean-field linear stability boundary of disordered phase in the $(\bar{m}, \varepsilon L_{\|})$ plane for three values of γ. The solid circles denote the "tricritical" point $\bar{m}_0$ defined via $g(1-\bar{m}_0, \gamma)=0$.

first order, this study yields at best the spinodal line. A similar stability analysis for the ordered phase is needed. If that state becomes unstable at the same points in the phase diagram, we can claim that a continuous transition is present. If the stability limits occur at another line, we would identify that line with the second spinodal, so that the first order transitions would be located in between the two spinodals. Unfortunately, such a linear stability analysis for the inhomogeneous state is considerably more arduous and remains to be performed.[24] In its absence, we can obtain some insight into the nature of the transitions by going beyond the terms linear in perturbations around the homogeneous state. In the next subsection we show the results of this approach, which exploits the method of adiabatic elimination[25] to project an equation of motion for the slow mode out of the full nonlinear dynamics (12).

4.4. Adiabatic Elimination of Fast Modes

Since we are interested in the limit $\tau_{-}(0, 2\pi/L_{\|}) \to 0$, we expect that there is only one slow mode, corresponding to this eigenvector of $\mathbb{L}$. Let us denote it symbolically by M; its precise definition will be given below. At the linear level all other modes will decay rapidly. Therefore, at the quadratic level [the only nonlinearity in (12)] the only modes with slow decay are those driven by M^2. Our analysis shows that there is only one such mode, which in turn is coupled back to M through a nonlinear term. The result is a nonlinear equation of motion for M alone. In this subsection we will give a few details of this approach.[25]

As we will be dealing with nonlinear contributions, we cannot make the same ansatz as in (20). Thus, we write the fields $\tilde{\phi}$, $\tilde{\psi}$, and ξ with their full time dependence. In Fourier space Eq. (12) now takes the form

$$\partial_t \xi(\mathbf{k}, t) = -\mathbb{L}(\mathbf{k})\, \xi(\mathbf{k}, t) + \mathsf{N}(\mathbf{k}; \{\xi(\mathbf{k}', t)\}) \tag{23a}$$

Here, $\mathsf{N}(\mathbf{k}; \{\xi(\mathbf{k}', t)\})$ is a two-component vector, quadratic in $\tilde{\phi}$ and $\tilde{\psi}$:

$$\mathsf{N}(\mathbf{k}; \{\xi(\mathbf{k}', t)\}) = \begin{bmatrix} N^{\phi}(\mathbf{k}; \{\xi(\mathbf{k}', t)\}) \\ N^{\psi}(\mathbf{k}; \{\xi(\mathbf{k}', t)\}) \end{bmatrix} \tag{23b}$$

with

$$N^{\phi}(\mathbf{k}; \{\xi(\mathbf{k}', t)\}) = -ik_{\|}\varepsilon \sum_{\mathbf{k}'} \tilde{\phi}(\mathbf{k}', t)\, \tilde{\psi}(\mathbf{k}-\mathbf{k}', t)$$

and

$$\begin{aligned} N^{\psi}(\mathbf{k}; \{\xi(\mathbf{k}', t)\}) = {} & (1-\gamma) \sum_{\mathbf{k}'} (\mathbf{k}' \mathbb{K} \mathbf{k}' - (\mathbf{k}-\mathbf{k}')\, \mathbb{K}(\mathbf{k}-\mathbf{k}'))\, \tilde{\phi}(\mathbf{k}', t) \tilde{\psi}(\mathbf{k}-\mathbf{k}', t) \\ & - ik_{\|}\varepsilon \left(1 - \frac{\gamma}{2}\right) \sum_{\mathbf{k}'} \tilde{\phi}(\mathbf{k}', t)\, \tilde{\phi}(\mathbf{k}-\mathbf{k}', t) \\ & - ik_{\|}\varepsilon \left(\frac{\gamma}{2}\right) \sum_{\mathbf{k}'} \tilde{\psi}(\mathbf{k}', t)\, \tilde{\phi}(\mathbf{k}-\mathbf{k}', t) \end{aligned} \tag{23c}$$

From the discussion in the previous paragraph, it is clear that we will never need to consider the $k_{\perp} \neq 0$ sector. Focusing only on longitudinal modes, we define, for short

$$\begin{gathered} \xi_m \equiv \xi\left(0, \frac{2\pi m}{L_{\|}}, t\right), \qquad \mathbb{L}_m \equiv \mathbb{L}\left(0, \frac{2\pi m}{L_{\|}}\right), \\ \mathsf{N}_m \equiv \mathsf{N}\left(0, \frac{2\pi m}{L_{\|}}; \{\xi(\mathbf{k}', t)\}\right) \end{gathered} \tag{24}$$

Note that, due to the reality of $\phi(\mathbf{r}, t)$ and $\psi(\mathbf{r}, t)$, $\xi_{-m} = \xi_m^*$.

In this notation the slow mode is part of $\xi_1(t)$. If we denote the eigenvectors of $\mathbb{L}_1$ by $\hat{e}_-$ and $\hat{e}_+$, associated with the eigenvalues $\tau_-(0, 2\pi/L_{\|})$ and $\tau_+(0, 2\pi/L_{\|})$, then the slow mode (M) can be identified through the decomposition

$$\xi_1(t) = M(t)\, \hat{e}_- + N(t)\, \hat{e}_+ \tag{25}$$

Explicitly,

$$\hat{e}_- \equiv \begin{bmatrix} 1 \\ 2\pi i/\varepsilon L_{||}\bar{\phi} \end{bmatrix} \tag{26}$$

By virtue of momentum conservation, we see from Eq. (23), that ξ_m couples only to $\xi_n \xi_{m-n}$ for all integer n. Near the transition we expect (the dominant parts of) all ξ_n with $n > 1$ to decay much faster than ξ_1. Therefore in the long-time limit we may neglect products of two ξ_n's with $n > 1$, and write

$$\partial_t \xi_1 \simeq -\mathbb{L}_1 \xi_1 + \mathsf{N}_1(\xi_1^*, \xi_2, 0, \ldots) \tag{27a}$$

for the $n = 1$ case. In the same spirit, the only $\xi_{n>1}$ which is coupled to the slow modes alone is the $n = 2$ case. Therefore, we may neglect all equations except for

$$\partial_t \xi_2 \simeq -\mathbb{L}_2 \xi_2 + \mathsf{N}_2(\xi_1, 0, 0, \ldots) \tag{27b}$$

Being a linear, though inhomogeneous, equation for ξ_2, it can be solved. In the long-time limit [i.e., t comparable to $1/\tau_-(O, 2\pi/L_{||})$ but much greater than the eigenvalues of $\mathbb{L}_2^{-1}$], the solution is $\mathbb{L}_2^{-1}\mathsf{N}_2(\xi_1, 0, 0, \ldots)$. Inserting this result into (27a), we obtain an equation of motion for ξ_1 only:

$$\partial_t \xi_1 \simeq -\mathbb{L}_1 \xi_1 + \mathsf{N}_1(\xi_1^*, +\mathbb{L}_2^{-1}\mathsf{N}_2(\xi_1, 0, 0, \ldots), 0, \ldots) \tag{28}$$

The final step consists in projecting (28) onto $\hat{e}_-$ in order to extract an equation for the slow mode. Some care has to be taken here because $\mathbb{L}_1$ is not Hermitian, so that the appropriate left eigenvector (i.e., conjugate of $\hat{e}_-$) must be computed. Meanwhile, since $\hat{e}_+$ is associated with a fast mode through the nonvanishing eigenvalue $\tau_+(O, 2\pi/L_{||})$, we may set $N(t) \simeq 0$ in the long-time limit. Thus, from (25), we may approximate $\xi_1(t)$ by $M(t)\,\hat{e}_-$ when inserted into (28) or (27b). The result, after tedious but straightforward algebra, is a Ginzburg–Landau type equation for $M(t)$:

$$\partial_t M = -\{\tau M + g\,|M|^2 M + O(M^5)\} \tag{29}$$

where $\tau \equiv \tau_-(O, 2\pi/L_{||})$ is the soft eigenvalue and g is a complicated function of ε, γ, $\bar{\phi}$, and $L_{||}$. Since (29) is of interest only near the stability limit, where $\tau \simeq 0$, we approximate ε by ε_{II} here. Using (22) to eliminate ε_{II} and $\bar{\phi} = 1 - i\bar{n}$, we obtain an explicit expression, up to an overall positive constant:

$$
\begin{aligned}
g \propto\ & [23(1-\gamma)^2(2-\gamma)^2]\,\bar{\phi}^4 \\
& + [30\gamma(1-\gamma)(2-\gamma)^2 - 44(1-\gamma)^3(2-\gamma)]\,\bar{\phi}^3 \\
& + [20(1-\gamma)^4 - 64\gamma(1-\gamma)^2(2-\gamma)]\,\bar{\phi}^2 \\
& + [32\gamma(1-\gamma)^3 - 6\gamma^2(1-\gamma)(2-\gamma)]\,\bar{\phi} \\
& + [5\gamma^2(1-\gamma)^2]
\end{aligned} \tag{30}
$$

We recognize (29) as the equation of motion for a dynamic model involving simple relaxation and the usual Landau–Ginzburg ϕ^4 Hamiltonian. Thus, the sign of g determines the order of the transition. If it is positive, the transition is continuous. On the other hand, $g<0$ is indicative that a first-order transition has presumably taken place *before* we arrive at this $\tau=0$ point. In the physical range $0<\bar{\phi}<1-\bar{m}_{\min}=(1-\gamma)/(2-\gamma)$ the (numerical) solution of (30) gives a unique zero for g at a critical hole density $\bar{\phi}_0(\gamma)$. Thus we predict a crossover from a first order to a continuous transition as the mass density $\bar{m}(\gamma)=1-\bar{\phi}(\gamma)$ increases beyond $\bar{m}_0(\gamma)$. One might label the point $(\bar{m}_0(\gamma), \varepsilon_H(\gamma, \bar{m}_0))$, marked by the solid circles in Fig. 9, as a nonequilibrium "tricritical" point. Keeping in mind however, that M is complex, we should refrain from drawing serious conclusions based on tricritical properties in known equilibrium systems.

For small γ, we find

$$
\bar{m}_0(\gamma) \simeq \frac{\sqrt{24}}{2(\sqrt{24}-1)} + 0.05\gamma + O(\gamma^2) \tag{31}
$$

indicating that $\bar{m}_0(\gamma)$ increases with γ, as borne out by the simulations. On the other hand, for $\gamma \to 1$, we observe that the "fraction" of the second-order region to the whole line, characterized by $R(\gamma) \equiv [1-\bar{m}_0(\gamma)]/[1-\bar{m}_{\min}(\gamma)]$ approaches the limit 5/6. So, intriguingly, even for γ very close to 1, mean-field theory predicts a small yet finite region of first order transitions, though these have not been observed in the simulations (Fig. 1). Two obvious possibilities for resolving this discrepancy is (a) that the transition is only weakly first order and (b) that they turn into continuous transitions once fluctuations are included in the theory.

5. CONCLUSIONS

We have investigated, by both Monte Carlo simulations and continuum mean-field theory techniques, the collective behavior of a system of two species of particles driven in opposite directions by an external

"electric" field E. In this sense, we regard the particles as being oppositely "charged." Extending earlier studies,[14-16] where particle–particle exchanges were prohibited, we allow such exchanges to occur at a fraction γ of the rate of particle–hole exchanges. As in the previous studies, square lattices with periodic boundary conditions are used. Also, the particles are non-interacting except for the excluded volume constraint, and the particle numbers of the two species are equal. Apart from γ and E, the remaining control parameter is the overall density of particles, $\bar{m}$.

Exploring in the range $\gamma \leqslant 1$, we seek transitions from a disordered phase with homogeneous densities and large currents to a "locked-up" phase characterized by inhomogeneous densities and small currents. First, we find a critical value $\gamma_c \simeq 0.62$ beyond which the system remains *disordered* for all $(\bar{m}, E)$. In contrast, for $\gamma < \gamma_c$ excluded volume effects dominate, so that the transition to ordered states occurs for sufficiently large $\bar{m}$ or E. A phase diagram is mapped out: a single sheet of transitions is present in the $(\bar{m}, E, \gamma)$ space. The nature of the transitions is first order on parts of this sheet and second order on other parts, with a line of multicritical points as the common boundary. To support these findings, we checked for discontinuities in the order parameters across the transitions and looked for the presence of hysteresis. Further, we compiled histograms and inquired whether the distributions remain single-peaked or develop second peaks. The fluctuations were also measured and their divergence with system size was noted qualitatively. Since we have not performed extensive finite-size analyses, we cannot present precise values for the various critical exponents, associated with the continuous transitions. Finally, we measured the profiles of both the hole and the charge densities in the ordered phase, emphasizing the characteristic differences between cases with $\gamma = 0$ and $\gamma \neq 0$.

Turning to analytic studies, we first derived a mean-field set of equations of motion for the two densities based on the master equation for our simple hopping model. We then demonstrated the existence of homogeneous and inhomogeneous stationary solutions to these equations, corresponding to the disordered and ordered phases respectively. The former follow trivially from conservation laws, while the latter can be found easily once the equations of motion have been recast in a form analogous to Newton's equation of motion for a particle in a potential. To confirm the presence of a transition between the two phases, we determined the linear stability boundary for the homogeneous solutions, noting that it mirrors the shape of the phase boundary rather well. In particular, the homogeneous phase was found to be stable for sufficiently large γ. The adiabatic elimination of the fast modes provided us with a Ginzburg–Landau type equation for the amplitude of the slow mode, thus giving us

some insight into the nature of the transitions: in agreement with the simulation data, the transitions are first order for small E and $\bar{m}$, turning second order as these parameters are increased beyond a multicritical point. Also, while the location of this point shifts to higher values of $\bar{m}$ as γ increases, the width of the first order region shrinks, approaching a finite fraction of the width of the whole transition region.

Finally, we conclude with some open questions and comments. While we have gained considerable insight into the finite-size and aspect-ratio dependence of the transition line throughout most of the phase diagram, the region near complete filling has not yet been explored in detail. It is here that the competition between ordering, mediated by the combination of bias and excluded volume constraints, and disordering, by virtue of charge exchange, may well be at its most subtle. Work is in progress to understand whether the transition line will meet the $\bar{m}-1$ line at some finite, γ-dependent E, or whether a finite region of disordered phase remains for all E. In the latter case, the system would display reentrant behavior.

A second interesting issue concerns the *universality class* of the continuous transitions. Again it will be paramount to understand the detailed finite-size and aspect-ratio dependence of the order parameters and their fluctuations. This analysis would be greatly simplified if field theory predictions of the associated critical exponents were available. The first step[23] toward the latter consists in adding appropriate noise terms to the mean-field equations (10), (12), proceeding to a full field theory for the slow mode $M(\mathbf{r}, t)$. Recalling the adiabatic elimination procedure, we see that any spatial dependence of M will be purely transverse. Our two-dimensional simulations will therefore be described by an effective theory in *one* (transverse) dimension which nevertheless exhibits a phase transition. There is clearly ample scope for further surprises in our simple model.

ACKNOWLEDGMENTS

We acknowledge K. E. Bassler, J. L. Lebowitz, H. Spohn, and Z. Toroczkai for many stimulating discussions and especially thank Z. Toroczkai for a critical reading of the manuscript. We are indebted to Z. Rácz and the organizers for their hospitality and support at the Eötvös Workshop, Budapest, July 1995, where this work was first presented. This research was supported in part by grants from the Division of Materials Research of the National Science Foundation and the Jeffress Memorial Trust.

REFERENCES

1. B. Schmittmann and R. K. P. Zia, In *Phase Transitions and Critical Phenomena*, Vol. 17, C. Domb and J. L. Lebowitz, eds. (Academic Press, New York, 1995).
2. S. Katz, J. L. Lebowitz, and H. Spohn, *Phys. Rev. B* **28**: 1655 (1983); *J. Stat. Phys.* **34**: 497 (1984).
3. P. C. Martin, E. D. Siggia, and H. H. Rose, *Phys. Rev. A* **8**: 423 (1973); H. K. Janssen, *Z. Phys. B* **23**: 377 (1976); C. de Dominicis, *J. Phys.* (Paris) *Colloq.* **37**: C247 (1976); R. Bausch, H. K. Janssen, and H. Wagner, *Z. Phys. B* **24**: 113 (1976).
4. H. K. Janssen and B. Schmittmann, *Z. Phys. B* **64**: 503 (1986). K.-T. Leung and J. L. Cardy, *J. Stat. Phys.* **44**: 567, 1087 (1986).
5. K. -t. Leung, *Phys. Rev. Lett.* **66**: 453 (1991); *Int. J. Mod. Phys. C* **3**: 367 (1992).
6. S. Chandra, *Superionic Solids. Principles and Applications* (North-Holland, Amsterdam, 1981).
7. M. Aertsens and J. Naudts, *J. Stat. Phys.* **62**: 609 (1990).
8. M. Rubinstein, *Phys. Rev. Lett.* **59**: 1946 (1987); T. A. J. Duke, *Phys. Rev. Lett.* **62**: 2877 (1989); Y. Shnidman, In *Mathematics in Industrial Problems IV*, A. Friedman, ed. (Springer, Berlin, 1991); B. Widom, J. L. Viovy, and A. D. Desfontaines, *J. Phys. I* (France) **1**: 1759 (1991).
9. O. Biham, A. A. Middleton, and D. Levine, *Phys. Rev. A* **46**: R6124 (1992); J. A. Cuesta, F. C. Martinez, J. M. Molera, and A. Sánchez, *Phys. Rev. E* **48**: R4176 (1993); K.-t. Leung, *Phys. Rev. Lett.* **73**: 2386 (1994); J. M. Molera, F. C. Martínez, and J. A. Cuesta, *Phys. Rev. E* **51**: 175 (1995).
10. R. B. Potts, *Proc. Camb. Phil. Soc.* **48**: 106 (1952); F. Y. Wu, *Rev. Mod. Phys.* **54**: 235 (1982).
11. J. Ashkin and E. Teller, *Phys. Rev.* **64**: 178 (1943).
12. M. Blume, V. J. Emery, and R. B. Griffiths, *Phys. Rev. A* **4**: 1071 (1971).
13. W. Selke, In *Phase Transitions and Critical Phenomena*, Vol. 15, C. Domb and J. L. Lebowitz, eds. (Academic Press, New York, 1993).
14. B. Schmittmann, K. Hwang, and R. K. P. Zia, *Europhys. Lett.* **19**: 19 (1992).
15. D. P. Foster and C. Godrèche, *J. Stat. Phys.* **76**: 1129 (1994).
16. K. E. Bassler, B. Schmittmann, and R. K. P. Zia, *Europhys. Lett.* **24**: 115 (1993).
17. V. Becker and H. K. Janssen, *Europhys. Lett.* **19**: 13 (1992).
18. B. Derrida, S. A. Janowsky, J. L. Lebowitz, and E. R. Speer, *Europhys. Lett.* **22**: 651 (1993); *J. Stat. Phys.* **73**: 813 (1993).
19. M. R. Evans, D. P. Foster, C. Godrèche, and D. Mukamel, *Phys. Rev. Lett.* **78**: 208 (1995); *J. Stat. Phys.* **80**: 69 (1995).
20. F. Spitzer, *Adv. Math.* **5**: 246 (1970).
21. G. Korniss, B. Schmittmann, and R. K. P. Zia, *Europhys. Lett.* **32**: 49 (1995).
22. I. Vilfan, R. K. P. Zia, and B. Schmittmann, *Phys. Rev. Lett.* **73**: 2071 (1994).
23. G. Korniss, B. Schmittmann, and R. K. P. Zia, to be published in *Physica A* (1997).
24. R. K. P. Zia and B. Schmittmann, Novel Goldstone modes in biased diffusion of two species, to be published.
25. H. Haken, *Synergetics, An Introduction*, 3rd ed. (Springer, Berlin, 1983).